Interplay of randomness, electron correlation, and dimensionality effects in quasi-one-dimensional conductors

Jun-ichiro Kishine[1] and Kenji Yonemitsu[1,2]

[1]*Department of Theoretical Studies, Institute for Molecular Science, Okazaki 444-8585, Japan*
[2]*Department of Functional Molecular Science, Graduate University for Advanced Studies, Okazaki 444-8585, Japan*
(Received 4 April 2000; revised manuscript received 12 June 2000)

We study the interplay of randomness, electron correlation, and dimensionality effects in weakly coupled half-filled Hubbard chains with weak quenched random potentials, based on the renormalization-group (RG) approach. We perform a two-loop RG analysis of an effective action derived by using the replica trick, and examine the following crossovers and phase transitions from an incoherent metal regime: (1) a crossover to the Anderson localization regime, (2) an antiferromagnetic phase transition, and (3) a crossover to the quasi-one-dimensional weak-localization regime. The case of $d = 1 + \epsilon$ ($\epsilon \ll 1$) dimensions is also mentioned.

I. INTRODUCTION

The interplay of randomness-driven Anderson localization and electron correlation has been a subject of controversy over the past two decades.[1-4] In $d = 2$ and 3 dimensions, coupling between two-particle scattering processes and diffusive motion of electrons (Cooperon) is treated perturbatively in the weak-localization regime, starting with the Fermi-liquid picture. On the other hand, in $d = 1$ dimension, coupling between two-particle scattering processes and random-potential scattering processes can never be treated perturbatively because of strong quantum fluctuations. Mutual renormalization effects of randomness and correlation in $d = 1$ have been treated through the renormalization-group approach based on the bosonization technique.[5,6] In the case of half-filling in $d = 1$, relevant $2k_F$ umklapp scattering causes a charge gap (Mott gap). Consequently, the interplay of randomness and correlation leads to competition between the Anderson localization and the Mott insulator phase.[7,8]

Because of the essential difference in nature between $d = 1$, 2, and 3 dimensions, the case of quasi-one-dimension is of particular interest. So far, discussions on a quasi-one-dimensional (Q1D) conductor with an open Fermi surface have been made in the *noninteracting* case, focused on weak-localization effects on conductivity[9] and magnetic-field effects on localization.[10-12] Little attention has been given to electron correlation effects in Q1D conductors with random potentials.

In the case of chains, without random potentials, weakly coupled via interchain one-particle hopping $t_\perp$, the system behaves as a 1D system at high energy (temperature) scales, $\omega \gg t_\perp$. As the energy decreases, there occurs interchain one-particle propagation through the $t_\perp$ process, and the propagation of the 1D power-law correlation through the interchain particle-hole or particle-particle exchange (ICEX) processes.[13-15] The former process induces one-particle crossover (1PC) to the Fermi-liquid regime, while the latter process converts the 1D power-law correlation to a 2D (or 3D) long-range correlation. Since the latter process occurs *irrespective of the interchain quasiparticle coherence*, a phase transition takes place from an ''incoherent metal

(ICM) regime,'' if the latter process dominates the former. We can confirm this scenario by using a renormalization-group (RG) approach based on the assumption that the scaling procedure in the one-dimensional regime at high-energy scales remains valid down to the phase transition or crossover energy scales. Competition between the ICEX-driven antiferromagnetic (AF) phase transition and the 1PC in half-filled[16,17] and dimerized quarter-filled[18] organic conductors have been investigated based on the RG approach, where relevant $2k_F$ umklapp scattering plays a key role for the ICEX-driven AF transition from the ICM regime.

In the case of weakly coupled half-filled chains with random potentials, it is also possible that the phase crosses over from the ICM regime to the Anderson localization (AL) regime.[19] It was recently reported that in a doped organic compound, $(DI\text{-}DCNQI)_2 Ag_{1-x} Cu_x$, where doping of Cu controls the dimensionality, randomness, and filling of the system, an AF ordering accompanied by a charge excitation gap (Mott gap), the Anderson localization regime, and a metal phase appear successively upon doping.[21] This experimental finding indicates that an interplay of correlation, randomness, and dimensionality is realized in this compound. In this paper, we extend work presented previously,[19] and study in detail an interplay of randomness, correlation, and dimensionality effects in the Q1D half-filled Hubbard system with weak quenched random potentials based on the RG approach. The effect of the varying filling is roughly simulated by changing the umklapp scattering strength. We consider weakly coupled chains, and treat the interchain one-particle hopping $t_\perp$ perturbatively to examine the consequent interchain one- and two-particle processes. Instead of the bosonization approach, we use the Grassmann functional integral approach in order to incorporate the interchain one-particle process explicitly. This approach is appropriate to obtain qualitative phase diagrams including a three-dimensionally ordered phase (the AF phase in the present case), but the feedback effects of the interchain processes on the intrachain processes are then missing. One way to retrieve the interchain feedback effects is to incorporate the imbalance between the elementary particle-particle (PP) and particle-hole (PH) loops: infrared logarithmic singularity of
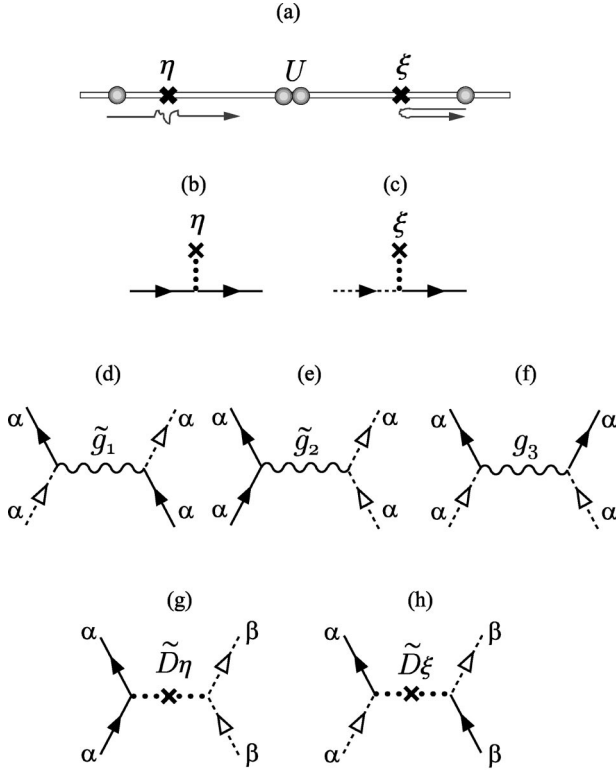
FIG. 1. (a) Half-filled Hubbard chain with random potentials considered here. (b) Forward and (c) backward scattering due to random potentials. (d) Backward, (e) forward, and (f) $2k_F$ umklapp scattering vertices. Inter-replica (g) forward and (h) backward scattering vertices. Solid and dashed lines represent one-particle propagators for right- and left-moving electrons, respectively.

the PH loop is smeared for $d>1$.[22] In the present paper, the $(d=1+\epsilon)$-dimensional case with randomness is taken up only briefly, because a fuller discussion was presented separately by one of the authors.[23]

This paper is organized as follows: In Sec. II, we consider an isolated half-filled Hubbard chain with weak quenched randomness. We construct an effective action via the replica trick, and apply a two-loop RG analysis to it. This part is a reformulation of the bosonization-based approach to the same problem.[6,7] In Sec. III, we extend the formulation presented in Sec. II to the case of the weakly coupled chains. Based on the RG flows, we introduce characteristic energy scales for the ICEX-driven AF transition, the crossover to the AL regime, and the 1PC, and discuss a low-energy asymptotic phase diagram of the system. The case of $d=1+\epsilon$ is discussed briefly in Sec. IV, followed by a summary in Sec. V.

II. SINGLE-CHAIN PROBLEM

We first consider an isolated half-filled Hubbard chain with weak quenched randomness [Fig. 1(a)].

A. Effective action

Here we construct an effective action via the replica trick. The following derivation is similar to that done by Belitz and Kirkpatrick.[4] We linearize the one-particle dispersion at the Fermi points $\pm k_F = \pm \pi/2$ as

$$\xi_\nu(k) = v_F(|k| - k_F). \tag{1}$$

Based on the bandwidth regularization scheme, we restrict the electron wave numbers to the region

$$\mathcal{C}_l = \{k| -\omega_l/2 \leqslant \xi_\nu(k) \leqslant \omega_l/2\}, \tag{2}$$

where $\xi_R(k) = v_F(k - k_F)$ $(k>0)$ and $\xi_L(k) = v_F(-k - k_F)$ $(k<0)$ are the linearized dispersions for the right- and left-moving electrons. The cutoff of the linearized band is parametrized as $\omega_l = E_0 e^{-l}$, with a scaling parameter l. The cutoff energy ω_l corresponds to a characteristic energy at which we observe the system. From now on we regard ω_l as the temperature scale $\omega_l \sim T$.

The renormalization-group procedure is best formulated in the path-integral representation of the partition function,

$$Z = \int_{\mathcal{C}_l} \mathcal{D} e^{S_l}, \tag{3}$$

where S_l is the effective action of the system, and $\mathcal{D}$ symbolizes the measure of the path integral over the fermionic Grassmann variables belonging to the region $\mathcal{C}_l$. The action at the energy scale specified by l contains four parts:

$$S_l = S_{\text{kin};l} + S_{\text{I};l} + S_{\eta;l} + S_{\xi;l}. \tag{4}$$

The kinetic action is given by

$$S_{\text{kin};l} = \sum_{k \in \mathcal{C}_l} \sum_{\varepsilon} \sum_{\sigma} [\mathcal{G}_R^{-1}(k) R_\sigma^*(k) R_\sigma(k) + \mathcal{G}_L^{-1}(k) L_\sigma^*(k) L_\sigma(k)], \tag{5}$$

where $k = (k, i\varepsilon)$, with ε being a fermion thermal frequency, and R_σ and L_σ are Grassmann variables representing the right- and left-moving electrons with a spin σ, respectively. The one-particle propagator is given by

$$\mathcal{G}_\nu(k) = [i\varepsilon - \xi_\nu(k)]^{-1}. \tag{6}$$

The two-particle scattering processes caused by the on-site repulsion [Fig. 1(a)] contain the normal and umklapp processes with the dimensionless scattering strengths, $g_{\sigma_1\sigma_2\sigma_3\sigma_4}$ and g_3, respectively. The corresponding term is written as

$$S_{\text{I};l} = \pi v_F T \sum_{\{k_i\} \in \mathcal{C}_l} \sum_{\{\varepsilon_i\}} \sum_{\{\sigma_i\}} g_{\sigma_1\sigma_2\sigma_3\sigma_4}$$
$$\times R_{\sigma_1}^*(k_1) L_{\sigma_2}^*(k_2) L_{\sigma_3}(k_3) R_{\sigma_4}(k_4)$$
$$-\frac{1}{2} \pi v_F g_3 T \sum_{\{k_i\} \in \mathcal{C}_l} \sum_{\{\varepsilon_i\}} \sum_{\sigma_1,\sigma_2} [R_{\sigma_1}^*(k_1) R_{\sigma_2}^*(k_2)$$
$$\times L_{\sigma_2}(k_3) L_{\sigma_1}(k_4) + \text{c.c}], \tag{7}$$

where T is absolute temperature, and the summation over energy and momentum is taken under the constraints $\varepsilon_1 + \varepsilon_2 - \varepsilon_3 - \varepsilon_4 = 0$ and $k_1 + k_2 - k_3 - k_4 = G$, with $G=0$ and $G = \pm 4k_F = \pm 2\pi$ for the normal and umklapp processes, respectively. The normal scattering is decomposed into backward and forward scattering as

$$g_{\sigma_1\sigma_2\sigma_3\sigma_4} = g_1 \delta_{\sigma_1\sigma_3} \delta_{\sigma_2\sigma_4} - g_2 \delta_{\sigma_1\sigma_4} \delta_{\sigma_2\sigma_3}, \tag{8}$$

where the forward and backward scattering strengths are denoted by g_2 and g_1, respectively. Unrenormalized scattering strengths are related to the on-site Coulomb repulsion U as

$$g_{1;0}=g_{2;0}=g_{3;0}=U/\pi v_F. \tag{9}$$

Scattering of electrons by the weak random potential [Fig. 1(a)] at a spatial position, x, is taken into account through a real field $\eta(x)$ corresponding to random forward scattering [Fig. 1(b)] and complex fields $\xi(x)$ and $\xi^*(x)$ corresponding to random backward scattering [Fig. 1(c)]. The corresponding actions are written as

$$S_{\eta;l}=-\int_0^{1/T} d\tau \int dx \sum_\sigma \eta(x)[R_\sigma^*(x,\tau)R_\sigma(x,\tau)$$
$$+L_\sigma^*(x,\tau)L_\sigma(x,\tau)], \tag{10}$$

$$S_{\xi;l}=-\int_0^{1/T} d\tau \int dx \sum_\sigma [\xi(x)R_\sigma^*(x,\tau)L_\sigma(x,\tau)$$
$$+\xi^*(x)L_\sigma^*(x,\tau)R_\sigma(x,\tau)]. \tag{11}$$

We assume the random potential to be governed by Gaussian distributions,

$$P_\eta \propto \exp\left[-D_\eta^{-1}\int dx\, \eta(x)^2\right],$$

$$P_\xi \propto \exp\left[-D_\xi^{-1}\int dx\, \xi(x)\xi^*(x)\right], \tag{12}$$

where $D_\eta=(\pi N_F\tau_\eta)^{-1}=v_F/\tau_\eta$ and $D_\xi=(\pi N_F\tau_\xi)^{-1}$ $=v_F/\tau_\xi$, with $\tau_{\eta,\xi}$ and N_F being the scattering mean free times and the noninteracting one-particle density of states, respectively. The correlation functions of the random potentials are then given by

$$\langle \eta(x)\eta(y)\rangle=\frac{D_\eta}{2}\delta(x-y), \quad \langle \xi(x)\xi^*(y)\rangle=\frac{D_\xi}{2}\delta(x-y). \tag{13}$$

In the case of quenched randomness, the free energy is averaged over random potentials by the replica trick, which is based on the identity

$$\ln Z=\lim_{N\to 0}\frac{Z^N-1}{N}. \tag{14}$$

By introducing N identical replicas of the system labeled by the index α, we obtain

$$Z^N=\int_{\mathcal{C}_l} \prod_{\alpha=1}^N \mathcal{D}_\alpha \exp\left[\sum_{\alpha=1}^N S_l^\alpha\right], \tag{15}$$

where $\mathcal{D}_\alpha$ symbolizes the measure of the path integral over the fermionic Grassmann variables in the αth replica. Then we take an average

$$\langle Z^N\rangle=\int d\eta P_\eta \int d\xi d\xi^* P_\xi \int_{\mathcal{C}_l} \prod_{\alpha=1}^N \mathcal{D}_\alpha \exp\left[\sum_{\alpha=1}^N S_l^\alpha\right]$$

$$\equiv \int_{\mathcal{C}_l} \prod_{\alpha=1}^N \mathcal{D}_\alpha \exp\left[\sum_{\alpha=1}^N \tilde{S}_l^\alpha\right] \tag{16}$$

for integer N, continue the result analytically to real N, and finally take the $N\to 0$ limit. Here $\tilde{S}_l^\alpha=\tilde{S}_{\text{kin};l}^\alpha+\tilde{S}_{\text{I};l}^\alpha+\tilde{S}_{\eta;l}^\alpha+\tilde{S}_{\xi;l}^\alpha$ is the replicated action corresponding to Eq. (4). $\tilde{S}_{\text{kin};l}^\alpha$ and $\tilde{S}_{\text{I};l}^\alpha$ are written simply by replacing R_σ and L_σ in Eqs. (5) and (7) with Grassman variables on the αth replica, R_σ^α and L_σ^α, respectively.

Performing the Gaussian integration over η and ξ fields, the forward and backward random scattering parts in the αth replica are obtained as follows:

$$\tilde{S}_{\eta;l}^\alpha=\frac{D_\eta}{2}\sum_{\beta=1}^N \sum_{\sigma_1,\sigma_2} \int_0^{1/T} d\tau_1 \int_0^{1/T} d\tau_2 \int dx R_{\sigma_1}^{\alpha*}(x,\tau_1)$$
$$\times R_{\sigma_1}^\alpha(x,\tau_1)L_{\sigma_2}^{\beta*}(x,\tau_2)L_{\sigma_2}^\beta(x,\tau_2), \tag{17}$$

$$\tilde{S}_{\xi;l}^\alpha=\frac{D_\xi}{2}\sum_{\beta=1}^N \sum_{\sigma_1,\sigma_2} \int_0^{1/T} d\tau_1 \int_0^{1/T} d\tau_2 \int dx R_{\sigma_1}^{\alpha*}(x,\tau_1)$$
$$\times L_{\sigma_1}^\alpha(x,\tau_1)L_{\sigma_2}^{\beta*}(x,\tau_2)R_{\sigma_2}^\beta(x,\tau_2). \tag{18}$$

To set up the RG equations, we need to pick up the logarithmically singular contribution originating from Eqs. (17) and (18). To do this, we change imaginary time variables τ_1 and τ_2 into $\Delta\tau=\tau_1-\tau_2$ and $\tau=(\tau_1+\tau_2)/2$, and introduce a short-distance cutoff Λ which characterizes the inelastic scattering regime between replicated systems. Then the region $v_F|\Delta\tau|\leq\Lambda$ causes an infrared logarithmic singularity, as the two-particle scattering processes (7) do, and contributes to the RG equations. Here we note that the condition $v_F|\Delta\tau|\leq\Lambda$ corresponds to the analogous one $v_F\Delta\tau\leq a$ in the bosonization-based formulation [see Eq. (3.2) of Ref. 6], where a is a short-distance cutoff parameter of the order of the lattice constant. We also note that elementary particle-hole and particle-particle loops for a fixed internal energy ε make contributions, $-\Sigma_{k\in\mathcal{C}_l}\mathcal{G}_R(k,\varepsilon)\mathcal{G}_L(k-2k_F,\varepsilon)=\Sigma_{k\in\mathcal{C}_l}\mathcal{G}_R(k,\varepsilon)\mathcal{G}_L(-k,-\varepsilon)=2\int_0^{E_0}[d\xi/(\xi^2+\varepsilon^2)]\sim\pi/\varepsilon$, for $\varepsilon\ll E_0$. The infrared logarithmic singularity comes from integration over the internal energy, $\int(d\varepsilon/\varepsilon)$, which we encounter only in the inelastic channel. From now on, we keep only the region $v_F|\Delta\tau|\leq\Lambda$ in Eqs. (17) and (18). Then, taking the Fourier transformation

$$R_\sigma^\alpha(\text{x})=T^{1/2}\sum_{k\in\mathcal{C}_l} \sum_\varepsilon e^{i(kx-\varepsilon\tau)}R_\sigma^\alpha(\text{k}),$$

$$R_\sigma^{\alpha*}(\text{x})=T^{1/2}\sum_{k\in\mathcal{C}_l} \sum_\varepsilon e^{-i(kx-\varepsilon\tau)}R_\sigma^{\alpha*}(\text{k}), \tag{19}$$

with $\text{x}=(x,\tau)$ and $\text{k}=(k,i\varepsilon)$, we have

$$\widetilde{S}^{\alpha}_{\eta;l} = \frac{D_{\eta}\Lambda}{v_F} T \sum_{\{k_i\}\in\mathcal{C}_l} \sum_{\{\varepsilon_i\}} \sum_{\sigma_1,\sigma_2} \sum_{\beta=1}^{N} R^{\alpha*}_{\sigma_1}(k_1)$$

$$\times L^{\beta*}_{\sigma_2}(k_2) L^{\beta}_{\sigma_2}(k_3) R^{\alpha}_{\sigma_1}(k_4), \tag{20}$$

$$\widetilde{S}^{\alpha}_{\xi;l} = -\frac{D_{\xi}\Lambda}{v_F} T \sum_{\{k_i\}\in\mathcal{C}_l} \sum_{\{\varepsilon_i\}} \sum_{\sigma_1,\sigma_2} \sum_{\beta=1}^{N} R^{\alpha*}_{\sigma_1}(k_1)$$

$$\times L^{\beta*}_{\sigma_2}(k_2) L^{\alpha}_{\sigma_1}(k_3) R^{\beta}_{\sigma_2}(k_4), \tag{21}$$

where the summation over energy and momentum is taken under the constraints: $\varepsilon_1+\varepsilon_2-\varepsilon_3-\varepsilon_4=0$ and $k_1+k_2-k_3-k_4=0$.

Now random scattering terms *inside the same replica* are absorbed into the intrachain two-particle scattering terms as

$$\widetilde{S}^{\alpha}_{I;l} = \pi v_F \widetilde{g}_1 T \sum_{\{k_i\}\in\mathcal{C}_l} \sum_{\{\varepsilon_i\}} \sum_{\sigma_1,\sigma_2} R^{\alpha*}_{\sigma_1}(k_1) L^{\alpha*}_{\sigma_2}(k_2) L^{\alpha}_{\sigma_1}(k_3)$$

$$\times R^{\alpha}_{\sigma_2}(k_4) - \pi v_F \widetilde{g}_2 T \sum_{\{k_i\}\in\mathcal{C}_l} \sum_{\{\varepsilon_i\}} \sum_{\sigma_1,\sigma_2} R^{\alpha*}_{\sigma_1}(k_1) L^{\alpha*}_{\sigma_2}(k_2)$$

$$\times L^{\alpha}_{\sigma_2}(k_3) R^{\alpha}_{\sigma_1}(k_4)$$

$$-\frac{1}{2}\pi v_F g_3 T \sum_{\{k_i\}\in\mathcal{C}_l} \sum_{\{\varepsilon_i\}} \sum_{\sigma_1,\sigma_2} [R^{\alpha*}_{\sigma_1}(k_1) R^{\alpha*}_{\sigma_2}(k_2)$$

$$\times L^{\alpha}_{\sigma_2}(k_3) L^{\alpha}_{\sigma_1}(k_4) + \text{c.c}], \tag{22}$$

where

$$\widetilde{g}_1 = g_1 - \widetilde{D}_{\xi}, \quad \widetilde{g}_2 = g_2 - \widetilde{D}_{\eta}, \tag{23}$$

$$\widetilde{D}_{\xi} = D_{\xi}\Lambda/\pi v_F^2, \quad \widetilde{D}_{\eta} = D_{\eta}\Lambda/\pi v_F^2. \tag{24}$$

The normal ($\widetilde{g}_1$ and $\widetilde{g}_2$) and the umklapp (g_3) scattering vertices are represented in Figs. 1(d), 1(e), and 1(f), respectively. On the other hand, random scattering terms *between different replicas* are written as

$$\widetilde{S}^{\alpha}_{\eta} = \pi v_F \widetilde{D}_{\eta} T \sum_{\{k_i\}\in\mathcal{C}_l} \sum_{\{\varepsilon_i\}} \sum_{\sigma_1,\sigma_2} \sum_{\beta\neq\alpha} R^{\alpha*}_{\sigma_1}(k_1) L^{\beta*}_{\sigma_2}(k_2)$$

$$\times L^{\beta}_{\sigma_2}(k_3) R^{\alpha}_{\sigma_1}(k_4), \tag{25}$$

$$\widetilde{S}^{\alpha}_{\xi} = -\pi v_F \widetilde{D}_{\xi} T \sum_{\{k_i\}\in\mathcal{C}_l} \sum_{\{\varepsilon_i\}} \sum_{\sigma_1,\sigma_2} \sum_{\beta\neq\alpha} R^{\alpha*}_{\sigma_1}(k_1) L^{\beta*}_{\sigma_2}(k_2)$$

$$\times L^{\alpha}_{\sigma_1}(k_3) R^{\beta}_{\sigma_2}(k_4), \tag{26}$$

where the corresponding inter-replica scattering vertices are represented in Figs. 1(g) and 1(h), respectively.

B. Two-loop renormalization

In the perturbative renormalization-group (PRG) approach, we assume that scattering strengths ($\widetilde{g}_1$, $\widetilde{g}_2$, g_3, $\widetilde{D}_{\eta}$, and $\widetilde{D}_{\xi}$) are considerably smaller than E_0, and set up low-order RG equations whose solutions indicate whether these small perturbations grow toward the low-energy scales or not. To discuss the interchain one-particle process in Sec.

III, we need to take account of the self-energy effects which are treated at the *two-loop* level. The derivation of the two-loop RG equations is left to Appendix A. The RG equations take the forms

$$d\widetilde{g}_1/dl = w_1 - 2\theta\widetilde{g}_1 - \widetilde{D}_{\xi}, \tag{27}$$

$$d\widetilde{g}_2/dl = w_2 - 2\theta\widetilde{g}_2 - \widetilde{D}_{\eta}, \tag{28}$$

$$dg_3/dl = w_3 - 2\theta g_3, \tag{29}$$

$$d\widetilde{D}_{\eta}/dl = w_{\eta} + (1-2\theta)\widetilde{D}_{\eta}, \tag{30}$$

$$d\widetilde{D}_{\xi}/dl = w_{\xi} + (1-2\theta)\widetilde{D}_{\xi}. \tag{31}$$

The self-energy processes give

$$\theta = \frac{1}{4}\left[\widetilde{g}_1^2 + \widetilde{g}_2^2 - \widetilde{g}_1\widetilde{g}_2 + \frac{1}{2}g_3^2 - \widetilde{D}_{\xi}^2 - \widetilde{D}_{\eta}^2\right], \tag{32}$$

and the vertex corrections give

$$w_1 = -\widetilde{g}_1^2 + \frac{1}{2}\widetilde{g}_1\widetilde{g}_2^2 - \frac{1}{2}\widetilde{g}_1^2\widetilde{g}_2 + \frac{1}{4}\widetilde{g}_1 g_3^2 + \widetilde{D}_{\xi}^2 - \frac{1}{2}\widetilde{g}_1\widetilde{D}_{\eta}^2, \tag{33}$$

$$w_2 = -\frac{1}{2}\widetilde{g}_1^2 + \frac{1}{2}g_3^2 + \frac{1}{2}\widetilde{g}_2^3 + \frac{1}{2}\widetilde{g}_1^2\widetilde{g}_2 - \frac{1}{2}\widetilde{g}_1\widetilde{g}_2^2 - \frac{1}{4}\widetilde{g}_1^3$$

$$+ \frac{1}{4}\widetilde{g}_1 g_3^2 - \frac{1}{4}\widetilde{g}_2 g_3^2 - \frac{1}{2}\widetilde{g}_2\widetilde{D}_{\eta}^2 + \frac{1}{2}\widetilde{D}_{\eta}\widetilde{D}_{\xi}^2, \tag{34}$$

$$w_3 = -\widetilde{g}_1 g_3 + 2\widetilde{g}_2 g_3 - \frac{1}{2}\widetilde{g}_2^2 g_3 + \frac{1}{2}\widetilde{g}_1\widetilde{g}_2 g_3$$

$$+ \frac{1}{4}\widetilde{g}_1^2 g_3 + \frac{1}{2}g_3\widetilde{D}_{\eta}^2, \tag{35}$$

$$w_{\eta} = \frac{1}{2}\widetilde{D}_{\xi}^2 + \frac{1}{2}\widetilde{g}_2^2\widetilde{D}_{\eta} + \frac{1}{2}\widetilde{g}_1^2\widetilde{D}_{\eta} - \frac{1}{2}\widetilde{g}_2\widetilde{D}_{\xi}^2 - \frac{1}{2}\widetilde{g}_1\widetilde{g}_2\widetilde{D}_{\eta}$$

$$+ \frac{1}{4}\widetilde{g}_1\widetilde{D}_{\xi}^2 - \frac{1}{4}g_3^2\widetilde{D}_{\eta} - \frac{1}{2}\widetilde{D}_{\eta}^3 - \frac{1}{2}\widetilde{D}_{\eta}\widetilde{D}_{\xi}^2, \tag{36}$$

$$w_{\xi} = -2\widetilde{g}_1\widetilde{D}_{\xi} + \widetilde{g}_2\widetilde{D}_{\xi} + \widetilde{D}_{\eta}\widetilde{D}_{\xi} - \widetilde{g}_2\widetilde{D}_{\eta}\widetilde{D}_{\xi} + \frac{1}{2}\widetilde{g}_1\widetilde{D}_{\eta}\widetilde{D}_{\xi}$$

$$-2\widetilde{D}_{\xi}^2 - \widetilde{D}_{\eta}^2\widetilde{D}_{\xi}. \tag{37}$$

C. RG flows and low-energy asymptotics of the single chain

Here we discuss the RG flows obtained through solutions of Eqs. (27)–(31) with initial values of the scattering strengths: $g_{1;0} = g_{2;0} = g_{3;0} = U/\pi v_F$, $\widetilde{D}_{\eta;0}$, and $\widetilde{D}_{\xi;0}$.

1. One-loop RG flows

To grasp qualitative nature of the RG flow, here we pause to look briefly at the one-loop counterparts of the RG equations:

$$d\widetilde{g}_1/dl = -\widetilde{D}_{\xi} - \widetilde{g}_1^2 + \widetilde{D}_{\xi}^2, \tag{38}$$
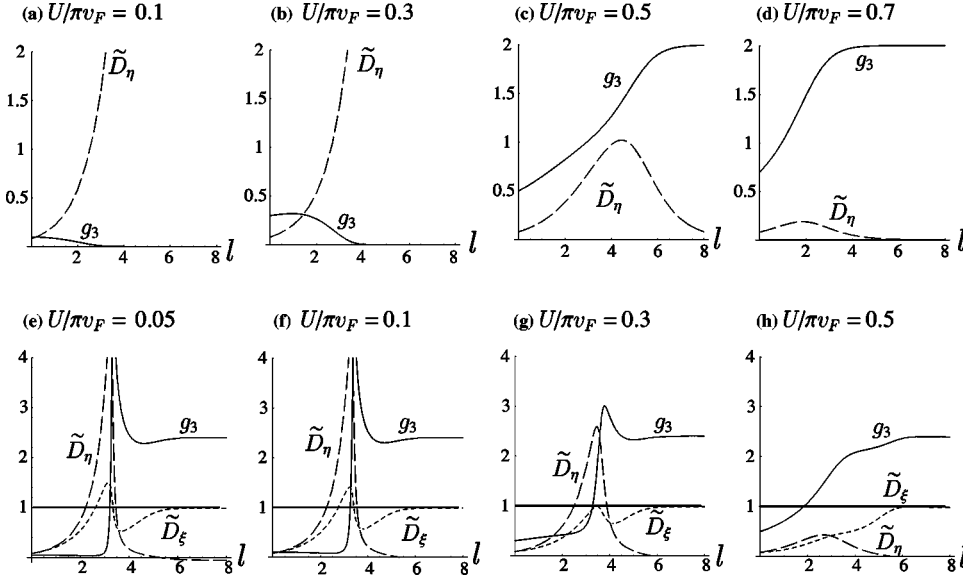
FIG. 2. Two-loop RG flows when the random forward scattering is present, but the random backward scattering is absent [(a)–(d)], and when both the random forward and backward scatterings are present [(e)–(h)].

$$d\widetilde{g}_2/dl = -\widetilde{D}_\eta - \widetilde{g}_1^2/2 + g_3^2/2, \qquad (39)$$

$$dg_3/dl = -g_3(\widetilde{g}_1 - 2\widetilde{g}_2), \qquad (40)$$

$$d\widetilde{D}_\eta/dl = \widetilde{D}_\eta + \widetilde{D}_\xi^2/2, \qquad (41)$$

$$d\widetilde{D}_\xi/dl = (1 - 2\widetilde{g}_1 + \widetilde{g}_2)\widetilde{D}_\xi + \widetilde{D}_\xi\widetilde{D}_\eta - 2\widetilde{D}_\xi^2. \qquad (42)$$

Case A: $\widetilde{D}_{\eta;0} \neq 0$ and $\widetilde{D}_{\xi;0} = 0$. When the random backward scattering is absent, the one-loop RG equations are reduced to

$$dG/dl = 2\widetilde{D}_\eta - g_3^2, \qquad (43)$$

$$dg_3/dl = -g_3 G, \qquad (44)$$

where $\widetilde{D}_\eta = \widetilde{D}_{\eta;0} e^l$ and $G = \widetilde{g}_1 - 2\widetilde{g}_2$. In this case, as seen from Eq. (43), $\widetilde{D}_\eta$ competes with g_3 and, consequently, the fixed points are classified into ($g_3^* = 0$, $G^* = \infty$, $\widetilde{D}_\eta^* = \infty$) and ($g_3^* = \infty$, $G^* = -\infty$, $\widetilde{D}_\eta^* = \infty$). This result is consistent with the finding by Fujimoto and Kawakami.[7] The former fixed point corresponds to the metal phase, where the random forward scattering overwhelms the umklapp scattering, while the latter corresponds to the Mott insulator phase.[7] For a fixed $\widetilde{D}_{\eta;0}$, a quantum phase transition occurs at some critical strength U_c, between the metal ($U < U_c$) and the Mott insulator ($U > U_c$) fixed points (for example, $U_c \sim 0.492\pi v_F$ for $\widetilde{D}_{\eta;0} = 0.08$).

Case B: $\widetilde{D}_{\eta;0} \neq 0$ and $\widetilde{D}_{\xi;0} \neq 0$. When both random forward and backward scatterings are present, the RG flows are modified, and the fixed points are classified into ($g_3^* = 0$, $G^* = \infty$, $\widetilde{D}_\eta^* = \infty$, $\widetilde{D}_\xi^* = \infty$) and ($g_3^* = \infty$, $G^* = -\infty$, $\widetilde{D}_\eta^* = \infty$, $\widetilde{D}_\xi^* = \infty$). The former fixed point corresponds to the Anderson insulator phase, while the latter corresponds to the Mott insulator phase.[7] For $\widetilde{D}_{\eta;0} = \widetilde{D}_{\xi;0} = 0.08$, a quantum phase transition takes place at $U_c \sim 0.439\pi v_F$ between the former ($U < U_c$) and the latter ($U > U_c$).

2. Two-loop RG flows

Next we discuss the two-loop RG flows obtained through solutions of Eqs. (27)–(31).

Case A: $\widetilde{D}_{\eta;0} \neq 0$ and $\widetilde{D}_{\xi;0} = 0$. In Figs. 2(a)–2(d), we show the flows for $U/\pi v_F = 0.1$, 0.3, 0.5, and 0.7, respectively, with $\widetilde{D}_{\eta;0} = 0.08$. The fixed points are classified into ($g_3^* = 0$, $G^* = \infty$, $\widetilde{D}_\eta^* = \infty$) and ($g_3^* = 2$, $G^* = -2$, $\widetilde{D}_\eta^* = 0$). The former fixed point is equivalent to the corresponding one-loop fixed point. On the other hand, the latter fixed point is equivalent to the nontrivial fixed point at the two-loop level,[24] corresponding to the pure Mott insulator. We thus see that two-loop analysis does not qualitatively modify the one-loop RG flows and, for a fixed $\widetilde{D}_{\eta;0}$, a quantum phase transition would occur at some critical strength U_c, between the metal and the Mott insulator fixed points (for example, $U_c \sim 0.484\pi v_F$ for $\widetilde{D}_{\eta;0} = 0.08$).

Case B: $\widetilde{D}_{\eta;0} \neq 0$ and $\widetilde{D}_{\xi;0} \neq 0$. The backward scattering qualitatively modifies the two-loop RG flows, and we find the fixed point ($g_3^* \sim 2.4003$, $G^* = -2.4349$, $\widetilde{D}_\eta^* = -0.0560$, $\widetilde{D}_\xi^* = 0.9844$) for *any* set of $U > 0$, $\widetilde{D}_{\eta;0}$, and $\widetilde{D}_{\xi;0}$. In Figs. 2(e)–2(h), we show the flows for $U/\pi v_F = 0.05$, 0.1, 0.3, and 0.5, respectively, with $\widetilde{D}_{\eta;0} = \widetilde{D}_{\xi;0} = 0.08$.

Now we introduce the characteristic scales l_{gap} and l_{loc} through the conditions $g_3 = 1$ at $l = l_{gap}$ and $\widetilde{D}_\xi = 1$ at $l = l_{loc}$. The corresponding energy scales, $E_{gap} = E_0 e^{-l_{gap}}$ and $E_{loc} = E_0 e^{-l_{loc}}$, can be regarded as characterizing the Mott gap opening and the Anderson localization, respectively. In Figs. 2(e)–2(h), we see that $l_{loc} < l_{gap}$ for smaller U, while $l_{loc} > l_{gap}$ for larger U. This behavior may indicate a crossover from the Anderson-insulator-like phase to the Mott-insulator-like phase upon increasing U.

The quantum critical behavior between two distinct fixed points, which is observed in the one-loop analysis, is apparently missing here. However, the fixed point found here is clearly out of the perturbative domain where the RG is valid and lies in the vicinity of the fixed point of the clean system. In fact, since at this fixed point $\widetilde{D}_\eta^* = -0.0560 < 0$, whereas by the definition of $\widetilde{D}_\eta$ [Eq. (13)], one must have $\widetilde{D}_\eta^* > 0$, the
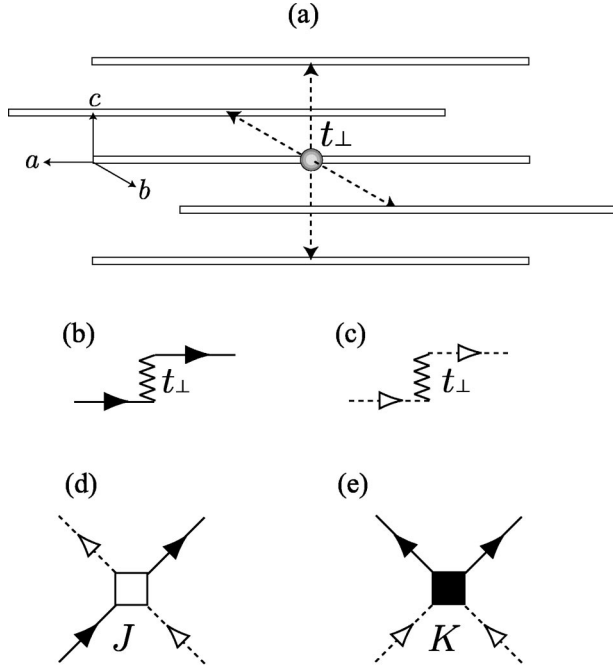
FIG. 3. (a) Three-dimensional regular array of parallel chains weakly coupled via the interchain one-particle hopping considered here. Interchain one-particle processes for (b) right- and (c) left-moving electrons. The interchain interaction in the antiferromagnetic channel classified into (d) normal and (e) umklapp processes.

field $\eta(x)$ being real, it is clear that the fixed point is an artifact of the two-loop RG. Thus we believe that the physics found by Fujimoto and Kawakami[7] at one-loop renormalization is not changed at two-loop renormalization.

III. WEAKLY COUPLED CHAINS

In this section, we consider a *three-dimensional* regular array of parallel chains weakly coupled via the interchain one-particle hopping $t_\perp$, as shown in Fig. 3(a), and examine the interchain one- and two-particle processes caused by $t_\perp$. *Here we stress that we deal with a three-dimensional system where infinitesimal random potentials do not induce Anderson localization.* We take the a axis in the direction parallel to the chains, and the b and c axes in directions perpendicular to the chains. The interchain one-particle hopping process between the nearest-neighbor chains causes a dispersion, $-2t_\perp(\cos k_b + \cos k_c)$. Throughout this section, we assume that the scaling procedure in the one-dimensional regime at high-energy scales ($\omega \gg t_\perp$) remains valid down to the energy scales at which the crossover or phase transition takes place.

A. Renormalization of the interchain processes

The action for the interchain one-particle process in the αth replica is written as

$$\tilde{S}^\alpha_{1\perp;l} = 2 \sum_{\substack{k_a \in C_l}} \sum_{-\pi \leqslant k_b, k_c \leqslant \pi} \sum_\varepsilon \sum_\sigma t_\perp (\cos k_b + \cos k_c)$$

$$\times [L^{\alpha*}_\sigma(K) L^\alpha_\sigma(K) + R^{\alpha*}_\sigma(K) R^\alpha_\sigma(K)], \quad (45)$$

where $K = (k_a, k_b, k_c, i\varepsilon)$, with k_a, k_b, and k_c the wave numbers along the a, b, and c axes, respectively. The corresponding one-particle processes are represented in Figs. 3(b) and 3(c).

By multiple use of the interchain one-particle processes and the intrachain two-particle processes, the interchain two-particle processes are dynamically generated during the renormalization.[13–15] We consider only the case where the most dominant correlation is an antiferromagnetic one. The corresponding term is written as

$$\tilde{S}^\alpha_{2\perp;l} = -\frac{\pi v_F T}{N_\perp} \sum_Q J_{q_\perp} S^\alpha_l(Q) \cdot S^\alpha_l(-Q)$$

$$-\frac{\pi v_F T}{N_\perp} \sum_Q K_{q_\perp} [S^\alpha_l(2k_F + q_a, q_\perp, i\omega)$$

$$\cdot S^\alpha_l(2k_F - q_a, -q_\perp, -i\omega) + \text{c.c}], \quad (46)$$

where $N_\perp$ is the number of chains and $Q = (q_a, q_\perp, i\omega)$, with $q_\perp = (q_b, q_c)$ and ω being a boson thermal frequency. $J_{q_\perp}$ and $K_{q_\perp}$ represent the strengths of the interaction between different chains through the normal and umklapp scattering, respectively [see Figs. 3(d) and 3(e)]. The $2k_F$ spin density is given by

$$S^\alpha_l(Q) = \sum_{\substack{k_a \in C_l \\ k_a + q_a \in C_l}} \sum_{-\pi \leqslant k_b, k_c \leqslant \pi} \sum_\varepsilon R^{\alpha*}_\sigma(K+Q)$$

$$\times \frac{\sigma_{\sigma\sigma'}}{2} L^\alpha_{\sigma'}(K). \quad (47)$$

Derivation of the RG equations for the interchain processes is left to Appendix B. We obtain the RG equations

$$d\ln t_\perp / dl = 1 - \theta, \quad (48)$$

$$dJ_{q_\perp} / dl = w^J_{q_\perp} - 2\theta J_{q_\perp}, \quad (49)$$

$$dK_{q_\perp} / dl = w^K_{q_\perp} - 2\theta K_{q_\perp}, \quad (50)$$

where

$$w^J_{q_\perp} = \frac{1}{2}(\tilde{g}_2^2 + 4g_3^2)(t_\perp / E_0)^2(\cos q_b + \cos q_c)$$

$$+ \frac{1}{2}(\tilde{g}_2 J_{q_\perp} + 4g_3 K_{q_\perp}) - \frac{1}{4}(J^2_{q_\perp} + 4K^2_{q_\perp}), \quad (51)$$

$$w^K_{q_\perp} = 2\tilde{g}_2 g_3 (t_\perp / E_0)^2(\cos q_b + \cos q_c)$$

$$+ 2(\tilde{g}_2 K_{q_\perp} + g_3 J_{q_\perp}) - J_{q_\perp} K_{q_\perp}. \quad (52)$$

We see that renormalization of the interchain one-particle process comes solely from the intrachain self-energy processes, where a nonuniversal exponent θ is given by Eq. (32). During the renormalization process, no new interchain one-particle hopping is generated. In Figs. 14(a) and 14(b) of Appendix B, we show contribution to $w^J_{q_\perp}$ and $w^K_{q_\perp}$, respectively. Although the unrenormalized values of $J_{q_\perp;0}$ and
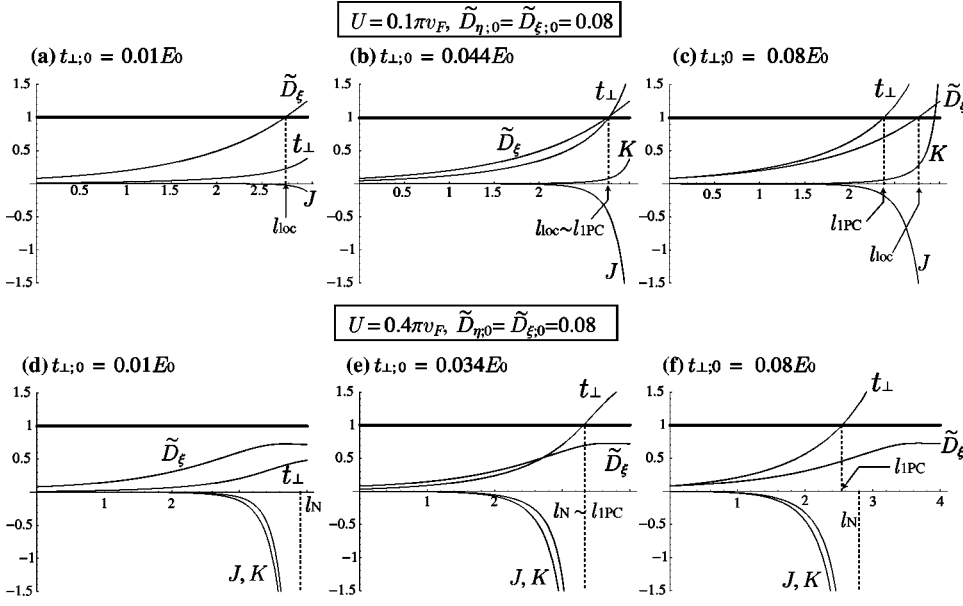
$U = 0.1\pi v_F, \ \tilde{D}_{\eta;0} = \tilde{D}_{\xi;0} = 0.08$

(a) $t_{\perp;0} = 0.01 E_0$ (b) $t_{\perp;0} = 0.044 E_0$ (c) $t_{\perp;0} = 0.08 E_0$

$U = 0.4\pi v_F, \ \tilde{D}_{\eta;0} = \tilde{D}_{\xi;0} = 0.08$

(d) $t_{\perp;0} = 0.01 E_0$ (e) $t_{\perp;0} = 0.034 E_0$ (f) $t_{\perp;0} = 0.08 E_0$

FIG. 4. RG flows of $t_\perp$, $\tilde{D}_\xi$, J, and K for $U = 0.1\pi v_F$ [(a)–(c)] and $U = 0.4\pi v_F$ [(d)–(f)].

$K_{q_\perp;0}$ are zero, the first terms of Eqs. (51) and (52), which come from the processes shown in Figs. 14(a-1) and 14(b-1) of Appendix B, respectively, generate finite magnitudes of $J_{q_\perp;0}$ and $K_{q_\perp;0}$. Then the second terms, which come from the processes shown in Figs. 14(a-2) and 14(b-2), respectively, induce their exponential growth. Finally the third terms, which come from the processes shown in Figs. 14(a-3) and 14(b-3), respectively, cause divergence of $J_{q_\perp}$ and $K_{q_\perp}$ at the critical scaling parameter l_c which depends on the momentum $q_\perp$ in the interchain direction. The divergence corresponds to the phase transition to the long-range ordered phase from the ICM regime at a temperature corresponding to $l_c(q_\perp)$. The most favorable spin-density-wave vector is given by the commensurate one, $q_\perp = Q_\perp^* = (\pi, \pi)$, at which the first terms of Eqs. (51) and (52) become negative and have maximum absolute values. From now on, we fix $q_\perp = Q_\perp^*$, and introduce $J = J_{Q_\perp^*}$, $K = K_{Q_\perp^*}$, and $l_N = l_c(Q_\perp^*)$. The temperature $T_N = E_0 e^{-l_N}$ gives the antiferromagnetic transition temperature. We note here that Eqs. (51) and (52) have the same form as those in the pure case,[17] except that g_1 and g_2 in the pure case are merely replaced with $\tilde{g}_1$ and $\tilde{g}_2$ [see Eq. (23)]. In the present formulation, *randomness effects on the interchain processes are incorporated through the modified intrachain two-particle scattering strengths, $\tilde{g}_1$ and $\tilde{g}_2$.*

B. RG flows and phase diagrams

Based on the RG flows obtained through solutions of Eqs. (27)–(31) and (48)–(50), we introduce the three characteristic scales, l_{loc}, l_{1PC}, and l_N:

$$\tilde{D}_\xi = 1 \quad \text{at} \quad l = l_{loc}, \tag{53}$$

$$t_\perp / E_0 = 1 \quad \text{at} \quad l = l_{1PC}, \tag{54}$$

$$J = K = -\infty \quad \text{at} \quad l = l_N. \tag{55}$$

Corresponding temperature scales are $T_{loc} = E_0 e^{-l_{loc}}$, $T_N = E_0 e^{-l_N}$, and $T_{1PC} = E_0 e^{-l_{1PC}}$. The scales l_{loc} and l_N, which

have already been introduced previously, characterize the crossover to the Anderson localization regime inside the ICM regime and the ICEX-driven AF phase transition from the ICM regime, respectively. The scale l_{1PC} gives a qualitative measure around which the one-particle crossover (1PC) occurs and interchain one-particle band motion begins to evolve.[25] Once the interchain one-particle band motion evolves, randomness effects may be treated as weak-localization corrections to the Q1D Fermi liquid (FL), as discussed by Abrikosov.[9] Thus we call this regime the Q1D weak-localization (Q1DWL) regime. We shall mention the weak-localization effects in the Q1D FL regime later in this subsection.

Here we stress again that we are dealing with a three-dimensional system where infinitesimal random potentials do not cause Anderson localization. This is what justifies the identification of the fixed point dominated by interchain hopping with a Fermi liquid. This identification is certainly invalid in two dimensions, where infinitesimal random potentials would still cause Anderson localization (AL).

We solve the coupled RG equations (27)–(31) and (48)–(50), and check which of Eqs. (53)–(55) is satisfied at the highest-energy scales (i.e., the smallest l). Here we fix initial strengths of the random scattering, $\tilde{D}_{\eta;0} = \tilde{D}_{\xi;0} = 0.08$. In Figs. 4(a)–4(c) are shown the RG flows of $t_\perp$, $\tilde{D}_\xi$, J, and K with $t_{\perp;0}/E_0 = 0.01$, 0.044, and 0.08, respectively, for $U = 0.1\pi v_F$. In this case, due to weaker U, growth of J and K is overwhelmed by growth of either $t_\perp$ or $\tilde{D}_\xi$, and consequently the low-temperature phases are determined by the competition between the AL and the 1PC. We see that the AL overwhelms the 1PC ($l_{loc} < l_{1PC}$) for $t_{\perp;0}/E_0 < 0.044$, while the 1PC overwhelms the AL ($l_{1PC} < l_{loc}$) for $t_{\perp;0}/E_0 > 0.044$.

In Figs. 4(d)–4(f) are shown the RG flows of $t_\perp$, $\tilde{D}_\xi$, J, and K with $t_{\perp;0}/E_0 = 0.01$, 0.034, and 0.08, respectively, for $U = 0.4\pi v_F$ and $\tilde{D}_{\eta;0} = \tilde{D}_{\xi;0} = 0.08$. In this case, due to stronger U, growth of $\tilde{D}_\xi$ is overwhelmed by growth of either $t_\perp$ or J or K, and consequently the low-temperature phases are determined by the competition between the AF transition and the 1PC. We see that the AF transition over-
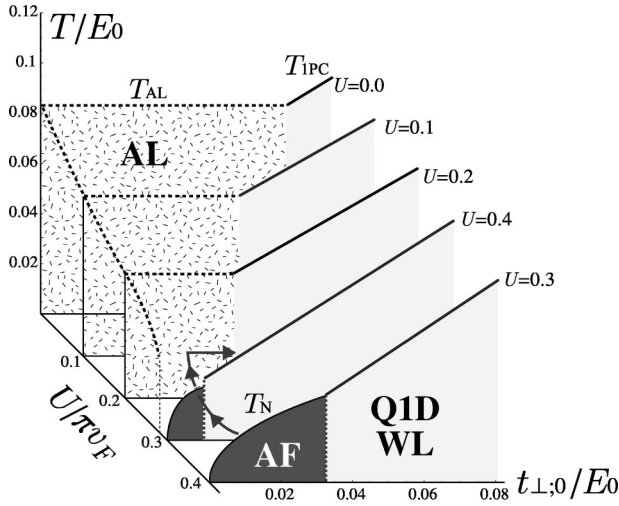
FIG. 5. Phase diagram spanned by $U/\pi v_F$, $t_{\perp;0}/E_0$, and the temperature scale T/E_0 for $\tilde{D}_{\eta;0} = \tilde{D}_{\xi;0} = 0.08$.

whelms the 1PC ($l_N < l_{1PC}$) for $t_{\perp;0}/E_0 < 0.034$, while the 1PC overwhelms the AF transition ($l_{1PC} < l_N$) for $t_{\perp;0}/E_0 > 0.034$.

By examining the RG flows for various U and $t_{\perp;0}$, we obtain a phase diagram spanned by $U/\pi v_F$ and $t_{\perp;0}/E_0$, and the temperature scale T/E_0 for $\tilde{D}_{\eta;0} = \tilde{D}_{\xi;0} = 0.08$, as shown in Fig. 5. We see that for very small $t_{\perp;0}$, the AL regime shrinks as U increases and the AF phases appears for $U/\pi v_F \gtrsim 0.28$. This crossover from the AL to AF phase is caused mainly by the increase of the umklapp scattering strength, which enhances the interchain AF correlation and suppresses the interchain one-particle process.[17,18]

In Fig. 6, we compare the cases with randomness ($\tilde{D}_{\eta;0} = \tilde{D}_{\xi;0} = 0.08$) and without randomness for $U/\pi v_F = 0.4$. We see that the AF transition temperature T_N in the case with randomness is suppressed as compared with the case without randomness. This suppression is mainly ascribed to suppression of the umklapp process due to the random forward scattering. It should be noted here that randomness effects may also remain in the AF phase. However, to clarify this issue,
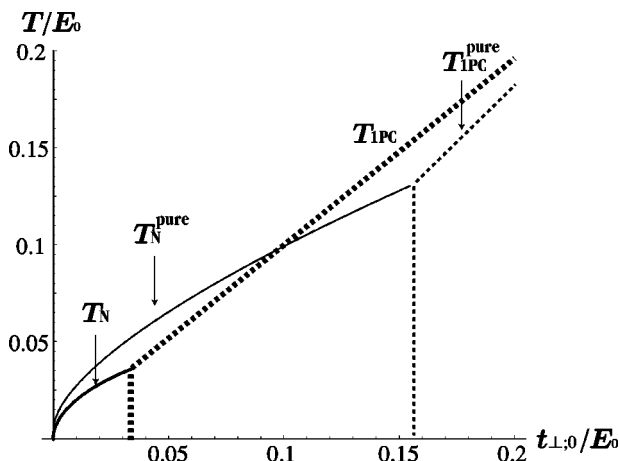

FIG. 6. The AF transition and 1PC temperatures in the cases with randomness, T_N and T_{1PC}, [$\tilde{D}_{\eta;0} = \tilde{D}_{\xi;0} = 0.08$], and without randomness, T_N^{pure} and T_{1PC}^{pure}, for $U/\pi v_F = 0.4$.
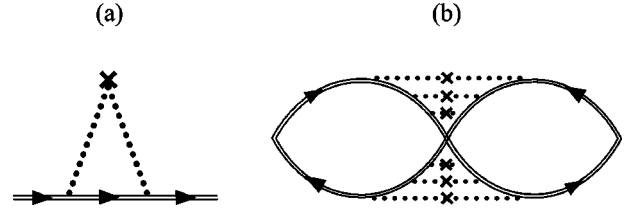

FIG. 7. (a) Self-energy processes caused by the random potentials. (b) Weak-localization correction to the classical conductivity. A double solid line represents the Q1D one-particle propagator $\mathcal{G}^{\text{Q1D}}$.

we need to go beyond the perturbative scheme, which is outside the scope of the present PRG approach.

Now let us briefly mention the weak-localization effects in the Q1DWL Fermi-liquid regime. For the present, we shall confine our attention to the noninteracting case. The present model gives the Q1D impurity-averaged propagator

$$\mathcal{G}^{\text{Q1D}}(\boldsymbol{k},\varepsilon) = [i\varepsilon - v_F(|k_a| - k_F) + 2t_\perp(\cos k_b + \cos k_c) + i\,\text{sgn}(\varepsilon)/2\tau]^{-1}, \quad (56)$$

where the inverse scattering time $\tau^{-1} = nv^2/v_F$ is caused by the self-energy processes, as shown in Fig. 7(a). Here n is the density of impurities, and v is the strength of the short-range random potential. Then the Cooperon propagator is obtained as

$$C(\boldsymbol{q},\omega) = nv^2[|\omega| + i\tau v_F q_a + 8\tau^2 t_\perp^2(\sin^2 q_b/2 + \sin^2 q_c/2)]^{-1}, \quad (57)$$

under the condition

$$v_F q_a \ll \tau^{-1}, \quad t_\perp \sin q_b/2 \ll \tau^{-1}, \quad t_\perp \sin q_c/2 \ll \tau^{-1}. \quad (58)$$

This condition justifies choosing the Cooperon diagrams as the main quantum correction to the conductivity. Then, we obtain the weak-localization correction [Fig. 7(b)] to the classical conductivity σ_0,

$$\Delta\sigma/\sigma_0 = -\tau^2 \int \frac{d\boldsymbol{q}}{(2\pi)^3} C(\boldsymbol{q},0), \quad (59)$$

where the integration is performed under condition (58). In the case where the warping of the Fermi surface is much larger than the broadening τ^{-1} due to the random scattering ($t_\perp \tau \gg 1$), the main contribution to $\Delta\sigma/\sigma_0$ comes from very small momenta,[9,12] $q_b, q_c \ll (t_\perp \tau)^{-1}$. Then, we obtain $\Delta\sigma/\sigma_0 \sim -(t_\perp \tau)^{-2}$, which is the same as that obtained by Abrikosov[9] in the case of the quadratic dispersion along the a axis. In the opposite case with $t_\perp \tau \ll 1$, we can integrate over q_b and q_c in the entire Brillouin zone, and obtain $\Delta\sigma/\sigma_0 \sim O(1)$, which indicates that the weak-localization picture breaks down. We see that the weak-localization picture on the randomness effects in the Q1D FL regime breaks down as $t_\perp \tau$ approaches unity from the side of $t_\perp \tau \gg 1$. The criteria $t_\perp \tau \sim 1$ may characterize a breakdown of the weak-localization regime from the side of the Fermi liquid.[9] This criteria may be consistent with the RG-based criteria $t_\perp/E_0$
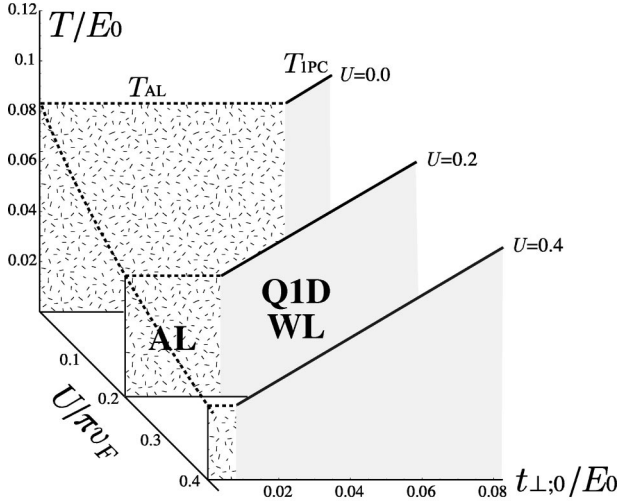
FIG. 8. Phase diagram in the case where the umklapp scattering is absent. The notations are the same as in Fig. 5.

$\sim \widetilde{D}_\xi = D_\xi \Lambda / \pi v_F^2 = (1/\pi v_F)(\Lambda / \tau_\xi)$, which characterizes the crossover from the AL regime to the Q1D regime from the one-dimensional side.

Here we consider the case sufficiently away from half filling, where the umklapp scattering is absent. In Fig. 8, we show a corresponding phase diagram spanned by $U/\pi v_F$ and $t_{\perp;0}/E_0$, and the temperature scale T/E_0 for $\widetilde{D}_{\eta;0} = \widetilde{D}_{\xi;0} = 0.08$. In this case the AL regime shrinks as U increases, but the AF phase never appears. Reduction of the localization temperature upon increasing U can be understood by the fact that repulsive interactions tend to make the charge density uniform, and thus compete with Anderson localization, as discussed in one dimension by Giamarchi and Shastry.[20] Comparing this result with that of Fig. 5, we see that the presence of the umklapp scattering is essential to cause the ICEX-driven AF transition from the ICM regime. This situation is similar to the case without randomness.[17,18]

C. AF phase, Anderson localization, and metallic phase in a doped organic compound (DI-DCNQI)$_2$Ag$_{1-x}$Cu$_x$

Here we mention an experimentally suggested phase diagram of a doped organic compound, (DI-DCNQI)$_2$Ag$_{1-x}$Cu$_x$,[21] where dimensionality, randomness, and filling vary upon doping. In the undoped case ($x = 0$), this compound consists of nearly isolated quarter-filled chains along the DCNQI columns and exhibits an AF ordering accompanied by the charge excitation gap.[26] Upon doping Cu, the filling decreases gradually from 1/4 ($x = 0$) down to 1/3 ($x = 1$), and dimensionality is raised by the increase of the interchain charge transfer via Cu sites. The degree of randomness caused by Cu substitution increases and decreases upon doping, with a maximum located around an intermediate doping region. Resistivity measurements indicate that the charge excitation gap rapidly collapses upon small doping, and then the Anderson localization phase appears at around a 48% doping of Cu, where three-dimensional variable range hopping is clearly observed. Upon further doping, dimensionality is raised, and the system exhibits metallic behavior down to low temperatures instead of localization.

The phase diagram (Fig. 5) may help account for this experimental finding on successive crossovers [AF→AL→ metallic phase] upon doping, although the present approach misses being correct in the following two respects. First, in actual (DI-DCNQI)$_2$Ag$_{1-x}$Cu$_x$, the charge localization for small x has been attributed to the relevant $4k_F$ umklapp process[27,28] instead of the $2k_F$ umklapp process at half-filling considered in this paper. The $4k_F$ umklapp process is not treated in the RG formulation unless we take higher-order scattering processes into account. In the present discussion, the presence of the $2k_F$ umklapp scattering is essential to cause an ICEX-driven AF transition from the ICM regime. We believe that this argument is applicable to the case of quarter-filling, where the relevant $4k_F$ umklapp scattering also suppresses the interchain one-particle process. Second, in actual (DI-DCNQI)$_2$Ag$_{1-x}$Cu$_x$, the closing of the charge gap may be attributed to changing the filling with fixed interaction strength, instead of changing the interaction strength with fixed filling. To explicitly change the filling, we should employ the approach used in Ref. 29, which is essentially equivalent to the bosonization-based approach in Ref. 30 in lowest order, although the cutoff functions are different in each case. To avoid further complexity, we would not employ this approach.

Keeping these points in mind, we try a simple simulation of the experimentally suggested successive crossovers. For small x, dimensionality is still low ($t_{\perp;0}$ is small), and the umklapp scattering may still survive at high-energy scales, but it may decrease upon doping. By simply assuming that U decreases as doping increases for small $t_{\perp;0}$, we simulate a crossover from the AF regime to the AL regime for small x. For further doping, $t_{\perp;0}$ may increase and the phase crosses over to the Q1DWL regime. We indicate these successive crossovers by the arrows in Fig. 5.

IV. CASE OF $d = 1 + \epsilon$ DIMENSIONS

It may be worth mentioning the $(d = 1 + \epsilon)$-dimensional case with randomness. Because fuller discussion on this topic is presented separately,[23] here we comment only briefly on the relevance to Sec. III. In Sec. III, we assumed that the scaling procedure in the one-dimensional regime at high-energy scales ($\omega \gg t_\perp$), where both the elementary particle-particle (PP) and particle-hole (PH) loops exhibit logarithmic singularities, remains valid down to the energy scale at which the crossover or phase transition takes place. Then we treated $t_\perp$ perturbatively to examine the interchain one- and two-particle processes caused by $t_\perp$. This approach is appropriate to obtain qualitative phase diagrams including a three-dimensionally ordered phase (the AF phase in the present case), but the feedback effects of the interchain processes on the charge gap formation are then missing. As a consequence, we cannot clarify the reason why the charge gap decreases as dimensionality is raised. One way to retrieve interchain feedback effects is to incorporate the imbalance between the PP and PH loops: the infrared logarithmic singularity of the PH loop is smeared for $d > 1$. One of the present authors studied the low-energy asymptotics of the $d = 1 + \epsilon$ ($\epsilon \ll 1$) dimensional Hubbard model with a circular Fermi surface where $2k_F$ umklapp scattering is present *a priori*.[23] Here we compare the $(d = 1 + \epsilon)$-dimensional case

with the case of the weakly coupled chains discussed in Sec. III.

In $d=1+\epsilon$, the real part of the elementary PP loop at the zero total momentum exhibits an infrared logarithmic singularity of the form

$$\mathrm{Re}\,\Delta_0(\omega) \sim -\frac{1}{2\pi v_F}\ln(\omega/E_0), \qquad (60)$$

where E_0 is the bandwidth cutoff. On the other hand, the real part of the elementary PH loop at $2k_F$ momentum transfer no longer exhibits an infrared singularity for $d>1$ and, in $d=1+\epsilon$, takes the form

$$\mathrm{Re}\,\Pi_{2k_F}(\omega) \sim \frac{1}{2\pi v_F}\left[\frac{\tilde{\omega}^{\epsilon/2}}{\epsilon/2}+C_\epsilon\right], \qquad (61)$$

where $\tilde{\omega}=\omega/2v_F k_F$ and C_ϵ is a constant independent of ω. By taking account of this imbalance between the PP and PH loops, and repeating similar procedures presented in Sec. II, we obtain the one-loop RG equations instead of the one-loop counterpart of Eqs. (27)–(31),[23]

$$\frac{d\tilde{g}_1}{dl} = -\tilde{D}_\xi - \tilde{g}_1\tilde{g}_2 + [(\tilde{g}_2-\tilde{g}_1)\tilde{g}_1+\tilde{D}_\xi^2]\lambda_l, \qquad (62)$$

$$\frac{d\tilde{g}_2}{dl} = -\tilde{D}_\eta - (\tilde{g}_1^2+\tilde{g}_2^2)/2 + (\tilde{g}_2^2+g_3^2)\lambda_l/2, \qquad (63)$$

$$\frac{dg_3}{dl} = -g_3(\tilde{g}_1-2\tilde{g}_2)\lambda_l, \qquad (64)$$

$$\frac{d\tilde{D}_\eta}{dl} = \tilde{D}_\eta + \tilde{D}_\xi^2/2, \qquad (65)$$

$$\frac{d\tilde{D}_\xi}{dl} = \tilde{D}_\xi + \tilde{D}_\xi\tilde{D}_\eta - [(2\tilde{g}_1-\tilde{g}_2)\tilde{D}_\xi+2\tilde{D}_\xi^2]\lambda_l, \qquad (66)$$

where the PH loop gives rise to the smooth cutoff[22]

$$\lambda_l \equiv 2\pi v_F\left|\frac{\partial}{\partial l}\mathrm{Re}\,\Pi_{2k_F}(\omega)\right| = \exp[-\epsilon l/2]. \qquad (67)$$

In this case, a quantum phase transition takes place from the Anderson insulator fixed point ($\tilde{D}_\xi^*=\infty$, $\tilde{D}_\eta^*=\infty$, $g_3^*=0$) to the Mott insulator fixed point ($\tilde{D}_\xi^*=\infty$, $\tilde{D}_\eta^*=\infty$, $g_3^*=\infty$) as $\tilde{U}$ increases.

In Fig. 9, we show a phase diagram spanned by $U/\pi v_F$, d, and the temperature scale T/E_0 for $\tilde{D}_{\eta;0}=\tilde{D}_{\xi;0}=0.08$, which corresponds to Fig. 5 in the case of weakly coupled chains. The definition of T_{loc} is the same as in Sec. III. The magnitude of the charge gap is qualitatively given by the energy scale, $\omega_{\mathrm{gap}}=E_0 e^{-l_{\mathrm{gap}}}$, at which the umklapp scattering strength exceeds unity; $g_3=1$.[18,31] In Fig. 9, we show the dependence of ω_{gap} on $U/\pi v_F$ and d. In $d=1+\epsilon$, both the three-dimensional AF phase transition and the one-particle crossover cannot be specified. Instead, the Mott insulator phase without the AF long-range order appears where the umklapp scattering g_3 overwhelms $\tilde{D}_\xi$. In $d=1$, a quantum phase transition from the AL regime to the Mott insulator
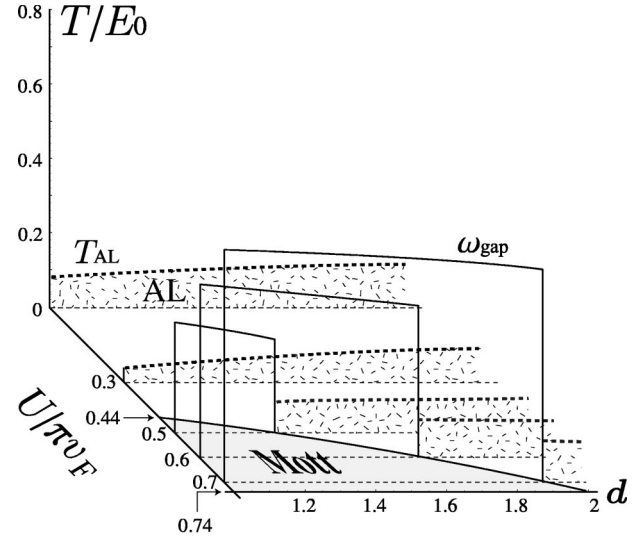

FIG. 9. Phase diagram spanned by $U/\pi v_F$, d, and the temperature scale T/E_0 for $\tilde{D}_{\eta;0}=\tilde{D}_{\xi;0}=0.08$.

phase occurs at $U/\pi v_F=0.44$. We see that ω_{gap} decreases as d increases for a fixed $U/\pi v_F$, indicating that the charge gap decreases as dimensionality increases.

In Fig. 10, we show a phase diagram in the case where the umklapp scattering is absent, which corresponds to Fig. 8 in the case of the weakly coupled chains. We see that T_{loc} decreases as a whole as U increases, but the AL regime is the only possible low-energy asymptotic phase.

V. SUMMARY

In this paper, we have studied the interplay of randomness, correlation, and dimensionality effects in the Q1D half-filled Hubbard system with weak quenched random potentials based on the RG approach. We first discussed chains weakly coupled via the interchain one-particle hopping $t_\perp$, using a two-loop RG analysis based on the assumption that the scaling procedure in the one-dimensional regime remains valid down to the energy scale at which the crossover or
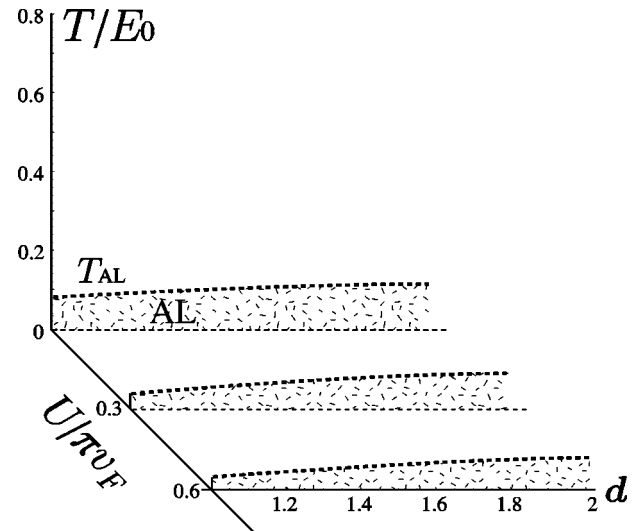

FIG. 10. Phase diagram in the case where the umklapp scattering is absent. The notations are the same as in Fig. 9.

phase transition occurs. We discussed the following cross-overs and phase transitions from the incoherent metal (ICM) regime: (1) the crossover to the Anderson localization (AL) regime; (2) the ICEX-driven antiferromagnetic (AF) phase transition; and (3) the crossover to the Q1D weak-localization regime (Q1DWL), where the randomness effects can be treated as weak-localization corrections to the Q1D Fermi liquid (FL). The main result is summarized in the phase diagram shown in Fig. 5. The presence of umklapp scattering is essential to cause an ICEX-driven AF transition from the ICM regime In the absence of umklapp scattering, only competition between crossovers to the AL regime and Q1DWL regime occurs (Fig. 8). Based on this result, we tried a simple simulation of the experimentally suggested successive crossovers (AF→AL→ metallic phase) upon doping in the organic compound, $(DI\text{-}DCNQI)_2Ag_{1-x}Cu_x$.[21] We also mentioned the $d=1 + \epsilon$ ($\epsilon \ll 1$) dimensional case.

ACKNOWLEDGMENTS

APPENDIX A: DERIVATION OF TWO-LOOP RG EQUATIONS IN SINGLE-CHAIN PROBLEM

In this section, we set up two-loop RG equations for the single-chain problem described by the effective action $\widetilde{S}_l^\alpha$.

We split up the set of k points $\mathcal{C}_l$ into two subsets as $\mathcal{C}_l = \mathcal{C}_{l+dl}^< \oplus d\mathcal{C}_{l+dl}^>$, where $\mathcal{C}_{l+dl}^< \equiv \{k \mid |\xi_\nu(k)| \leq \omega_{l+dl}/2\}$ and $d\mathcal{C}_{\nu;l+dl}^> \equiv \{k \mid \omega_{l+dl}/2 \leq |\xi_\nu(k)| \leq \omega_l/2\}$ represent the low- and high-energy shells, respectively. Accordingly, the action is decomposed as $\widetilde{S}_l = \widetilde{S}_{l+dl}^< + \widetilde{S}_{l+dl}^>$. Integration over the modes in the high-energy shell gives

$$Z = \int_{\mathcal{C}_{l+dl}^<} \prod_{\alpha=1}^N \mathcal{D}_\alpha \exp\left[\sum_{\alpha=1}^N \left\{ \widetilde{S}_{l+dl}^{\alpha<} + \sum_{p,q,r=1}^\infty dS_{pqr}^\alpha \right\}\right].$$
(A1)

All the renormalization effects come from the perturbative expansion,

$$dS_{pqr}^\alpha = \frac{1}{p!q!r!} \ll [\widetilde{S}_{I;l+dl}^{\alpha>}]^p [\widetilde{S}_{\eta;l+dl}^{\alpha>}]^q [\widetilde{S}_{\xi;l+dl}^{\alpha>}]^r \gg_c,$$
(A2)

where $\int_{\mathcal{C}_{l+dl}^<} \prod_{\alpha=1}^N \mathcal{D}_\alpha$ means that the fermion momenta are restricted to the low-energy shell. The average over the modes in the high-energy shell is defined as $\ll(\cdots)\gg = Z_>^{-1} \int_{d\mathcal{C}_{l+dl}^>} \prod_{\alpha=1}^N \mathcal{D}_\alpha \exp[\widetilde{S}_{kin;l+dl}^{\alpha>}](\cdots)$, with $Z_> = \int_{d\mathcal{C}_{l+dl}^>} \prod_{\alpha=1}^N \mathcal{D}_\alpha \exp[\widetilde{S}_{kin;l+dl}^{\alpha>}]$, and the subscript c represents the connected diagrams. We perform a perturbative expansion by picking up the Feynmann diagrams whose contribution is in proportion to dl. Note that diagrams in proportion to dl give rise to the corresponding logarithmic singularity as $\int_0^l dl' = l = \ln(E_0/\omega_l)$. Then the renormalized action is written in the form

$$\widetilde{S}_{l+dl}^{\alpha<} + \sum_{p,q,r=1}^\infty dS_{pqr}^\alpha = \sum_{k \in \mathcal{C}_{l+dl}} \sum_\varepsilon \sum_\sigma (1+\theta dl)[\mathcal{G}_R^{-1}(k)R_\sigma^{\alpha*}(k)R_\sigma^\alpha(k) + \mathcal{G}_L^{-1}(k)L_\sigma^{\alpha*}(k)L_\sigma^\alpha(k)]$$

$$+ \pi v_F(\widetilde{g}_1 + w_1 dl)T \sum_{\{k_i\} \in \mathcal{C}_{l+dl}} \sum_{\{\varepsilon_i\}} \sum_{\sigma_1,\sigma_2} R_{\sigma_1}^{\alpha*}(k_1)L_{\sigma_2}^{\alpha*}(k_2)L_{\sigma_1}^\alpha(k_3)R_{\sigma_2}^\alpha(k_4)$$

$$- \pi v_F(\widetilde{g}_2 + w_2 dl)T \sum_{\{k_i\} \in \mathcal{C}_{l+dl}} \sum_{\{\varepsilon_i\}} \sum_{\sigma_1,\sigma_2} R_{\sigma_1}^{\alpha*}(k_1)L_{\sigma_2}^{\alpha*}(k_2)L_{\sigma_2}^\alpha(k_3)R_{\sigma_1}^\alpha(k_4)$$

$$- \frac{1}{2}\pi v_F(g_3 + w_3 dl)T \sum_{\{k_i\} \in \mathcal{C}_{l+dl}} \sum_{\{\varepsilon_i\}} \sum_{\sigma_1,\sigma_2} [R_{\sigma_1}^{\alpha*}(k_1)R_{\sigma_2}^{\alpha*}(k_2)L_{\sigma_2}^\alpha(k_3)L_{\sigma_1}^\alpha(k_4) + c.c]$$

$$+ \pi v_F(\widetilde{D}_\eta + w_\eta dl)T \sum_{\{k_i\} \in \mathcal{C}_{l+dl}} \sum_{\{\varepsilon_i\}} \sum_{\sigma_1,\sigma_2} \sum_{\beta \neq \alpha} R_{\sigma_1}^{\alpha*}(k_1)L_{\sigma_2}^{\beta*}(k_2)L_{\sigma_2}^\beta(k_3)R_{\sigma_1}^\alpha(k_4)$$

$$- \pi v_F(\widetilde{D}_\xi + w_\xi dl)T \sum_{\{k_i\} \in \mathcal{C}_{l+dl}} \sum_{\{\varepsilon_i\}} \sum_{\sigma_1,\sigma_2} \sum_{\beta \neq \alpha} R_{\sigma_1}^{\alpha*}(k_1)L_{\sigma_2}^{\beta*}(k_2)L_{\sigma_1}^\alpha(k_3)R_{\sigma_2}^\beta(k_4).$$
(A3)

Note that $\{k_i\} \in \mathcal{C}_{l+dl}$ here, instead of $\{k_i\} \in \mathcal{C}_l$ in Eqs. (5)–(26).

Next, to restore the original cutoff, we rescale the momenta and frequencies as

$$\hat{k} = e^{dl}k,$$
(A4)

and perform the field renormalization

$$\hat{R}(\hat{k}) = \left(1 + \frac{\theta-3}{2}dl\right)R(k)$$
(A5)

to keep the kinetic action scale-invariant. We must bear in mind that the length scale Λ contained in the random scattering strengths ($\widetilde{D}_\eta$ and $\widetilde{D}_\xi$) is also rescaled to $\Lambda e^{dl} = \Lambda + \Lambda dl$. Then the renormalized action (A3) takes the form

$$\sum_{\hat{k}\in\mathcal{C}_l}\sum_{\hat{\varepsilon}}\sum_{\sigma}[\mathcal{G}_R^{-1}(\hat{k})\hat{R}_\sigma^{\alpha*}(\hat{k})\hat{R}_\sigma^\alpha(\hat{k})+\mathcal{G}_L^{-1}(\hat{k})\hat{L}_\sigma^{\alpha*}(\hat{k})\hat{L}_\sigma^\alpha(\hat{k})]$$

$$+\pi v_F[\tilde{g}_1+(w_1-2\theta\tilde{g}_1-\tilde{D}_\xi)dl]\hat{T}\sum_{\{\hat{k}_i\}\in\mathcal{C}_l}\sum_{\{\hat{\varepsilon}_i\}}\sum_{\sigma_1,\sigma_2}\hat{R}_{\sigma_1}^{\alpha*}(\hat{k}_1)\hat{L}_{\sigma_2}^{\alpha*}(\hat{k}_2)\hat{L}_{\sigma_1}^\alpha(\hat{k}_3)\hat{R}_{\sigma_2}^\alpha(\hat{k}_4)$$

$$-\pi v_F[\tilde{g}_2+(w_2-2\theta\tilde{g}_2-\tilde{D}_\eta)dl]\hat{T}\sum_{\{\hat{k}_i\}\in\mathcal{C}_l}\sum_{\{\hat{\varepsilon}_i\}}\sum_{\sigma_1,\sigma_2}\hat{R}_{\sigma_1}^{\alpha*}(\hat{k}_1)\hat{L}_{\sigma_2}^{\alpha*}(\hat{k}_2)\hat{L}_{\sigma_2}^\alpha(\hat{k}_3)\hat{R}_{\sigma_1}^\alpha(\hat{k}_4)$$

$$-\frac{1}{2}\pi v_F[g_3+(w_3-2\theta g_3)dl]\hat{T}\sum_{\{\hat{k}_i\}\in\mathcal{C}_l}\sum_{\{\hat{\varepsilon}_i\}}\sum_{\sigma_1,\sigma_2}[\hat{R}_{\sigma_1}^{\alpha*}(\hat{k}_1)\hat{R}_{\sigma_2}^{\alpha*}(\hat{k}_2)\hat{L}_{\sigma_2}^\alpha(\hat{k}_3)\hat{L}_{\sigma_1}^\alpha(\hat{k}_4)+\text{c.c}]$$

$$+\pi v_F[\tilde{D}_\eta+\{w_\eta+(1-2\theta)\tilde{D}_\eta\}dl]\hat{T}\sum_{\{\hat{k}_i\}\in\mathcal{C}_l}\sum_{\{\hat{\varepsilon}_i\}}\sum_{\sigma_1,\sigma_2}\sum_{\beta\neq\alpha}\hat{R}_{\sigma_1}^{\alpha*}(\hat{k}_1)\hat{L}_{\sigma_2}^{\beta*}(\hat{k}_2)\hat{L}_{\sigma_2}^\beta(\hat{k}_3)\hat{R}_{\sigma_1}^\alpha(\hat{k}_4)$$

$$-\pi v_F[\tilde{D}_\xi+\{w_\xi+(1-2\theta)\tilde{D}_\xi\}dl]\hat{T}\sum_{\{\hat{k}_i\}\in\mathcal{C}_l}\sum_{\{\hat{\varepsilon}_i\}}\sum_{\sigma_1,\sigma_2}\sum_{\beta\neq\alpha}\hat{R}_{\sigma_1}^{\alpha*}(\hat{k}_1)\hat{L}_{\sigma_2}^{\beta*}(\hat{k}_2)\hat{L}_{\sigma_1}^\alpha(\hat{k}_3)\hat{R}_{\sigma_2}^\beta(\hat{k}_4). \tag{A6}$$

Note that $\{\hat{k}_i\}\in\mathcal{C}_l$ here again, and the original cutoff has been restored. By identifying the quantities in brackets $[\cdots]$ in the second to sixth lines with the renormalized scattering strengths, we obtain the RG equations in the form of Eqs. (27)–(31).

We evaluate θ, w_1, w_2, w_3, w_η, and w_ξ at the two-loop level. The self-energy diagrams which contribute to θ are shown in Figs. 11(a)–11(d). Since the contribution of the diagrams containing a loop connected via the random scattering to outer lines, as shown in Fig. 11(e), is proportional to the number of replicas, N, and vanishes in the replica limit $N\to 0$, we subtract the contribution of Figs. 11(a′) and 11(b′), which are fictitiously counted in Figs. 11(a) and 11(b), respectively. Thus we obtain

$$\theta=\frac{1}{4}\left[\tilde{g}_1^2+\tilde{g}_2^2-\tilde{g}_1\tilde{g}_2+\frac{1}{2}g_3^2-\tilde{D}_\eta^2-\tilde{D}_\xi^2\right]. \tag{A7}$$

The first, second, ..., sixth terms of the right-hand side come from Figs. 11(a), 11(b), ..., 11(d), 11(a′), and 11(b′), respectively.

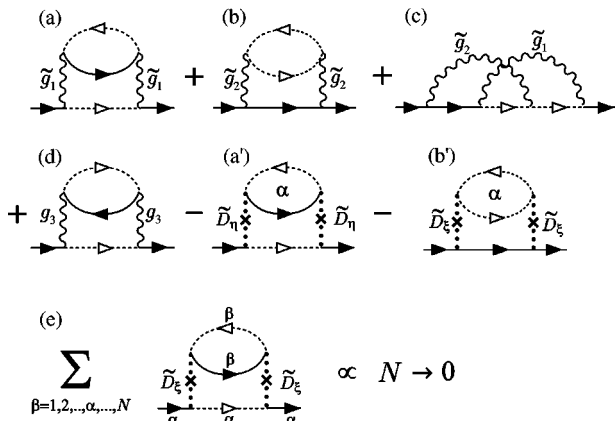
(a)   (b)   (c)   (d)   (a′)   (b′)

(e)

$$\sum_{\beta=1,2,..,\alpha,...,N}$$ $\propto$ $N\to 0$

FIG. 11. (a)–(d), (a′) and (b′) are the self-energy diagrams which contribute to θ. Diagram (e) is proportional to the number of replicas N, and vanishes in the replica limit $N\to 0$.

The diagrams which contribute to w_1 are shown in Fig. 12(a-1)–12(a-4). We subtract contribution Fig. 12(a-1′) and 12(a-2′), which are fictitiously counted in Fig. 12(a-1) and 12(a-2), respectively. Thus we obtain

$$w_1=-\tilde{g}_1^2+\frac{1}{2}\tilde{g}_1\tilde{g}_2^2-\frac{1}{2}\tilde{g}_1^2\tilde{g}_2+\frac{1}{4}\tilde{g}_1g_3^2+\tilde{D}_\xi^2-\frac{1}{2}\tilde{g}_1\tilde{D}_\eta^2. \tag{A8}$$

The first, second, ..., sixth terms of the right-hand side come from Figs. 12(a-1)–12(a-4), 12(a-1′), and 12(a-2′), respectively.

The diagrams which contribute to w_2 are shown in Figs. 12(b-1)–12(b-8). We subtract contribution of Figs. 12(b-3′) and 12(b-4′), which are fictitiously counted in Figs. 12(b-3) and 12(b-4), respectively. Thus we obtain

$$w_2=-\frac{1}{2}\tilde{g}_1^2+\frac{1}{2}g_3^2+\frac{1}{2}\tilde{g}_2^3+\frac{1}{2}\tilde{g}_1^2\tilde{g}_2-\frac{1}{2}\tilde{g}_1\tilde{g}_2^2-\frac{1}{4}\tilde{g}_1^3+\frac{1}{4}\tilde{g}_1g_3^2$$
$$-\frac{1}{4}\tilde{g}_2g_3^2-\frac{1}{2}\tilde{g}_2\tilde{D}_\eta^2+\frac{1}{2}\tilde{D}_\eta\tilde{D}_\xi^2. \tag{A9}$$

The first, second, ..., tenth terms of the right-hand side come from Figs. 12(b-1), ..., 12(b-8), 12(b-3′), and 12(b-4′), respectively. Two diagrams labeled in Fig. 12(b-8) give the eighth term.

The diagrams which contribute to w_3 are shown in Figs. 12(c-1)–12(c-5). We subtract contribution of Fig. 12(c-3′), which is fictitiously counted in Fig. 12(c-3). Thus we obtain

$$w_3=-\tilde{g}_1g_3+2\tilde{g}_2g_3-\frac{1}{2}\tilde{g}_2^2g_3+\frac{1}{2}\tilde{g}_1\tilde{g}_2g_3$$
$$+\frac{1}{4}\tilde{g}_1^2g_3+\frac{1}{2}g_3\tilde{D}_\eta^2. \tag{A10}$$

The first, second, ..., sixth terms of the right-hand side come from Figs. 12(c-1), ..., 12(c-5) and 12(c-3′), respectively.

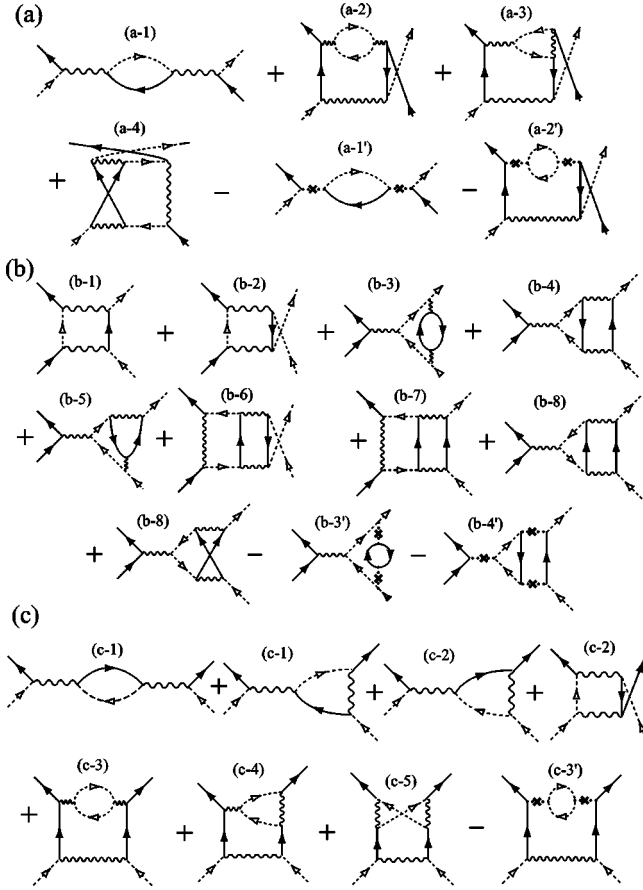FIG. 12. Vertex correction diagrams which contribute to (a) w_1, (b) w_2, and (c) w_3.

The diagrams which contribute to w_η are shown in Figs. 13(a-1)–13(a-7). We subtract contribution of Figs. 13(a-2') and 13(a-3'), which are fictitiously counted in Figs. 13(a-2) and 13(a-3), respectively. Thus we obtain

$$w_\eta = \frac{1}{2}\tilde{D}_\xi^2 + \frac{1}{2}\tilde{g}_2^2\tilde{D}_\eta + \frac{1}{2}\tilde{g}_1^2\tilde{D}_\eta - \frac{1}{2}\tilde{g}_2\tilde{D}_\xi^2 - \frac{1}{2}\tilde{g}_1\tilde{g}_2\tilde{D}_\eta$$

$$+ \frac{1}{4}\tilde{g}_1\tilde{D}_\xi^2 - \frac{1}{4}g_3^2\tilde{D}_\eta - \frac{1}{2}\tilde{D}_\eta^3 - \frac{1}{2}\tilde{D}_\eta\tilde{D}_\xi^2. \tag{A11}$$

The first, second, . . . , ninth terms of the right-hand side come from Figs. 13(a-1), . . . , 13(a-7), 13(a-2'), and 13(a-3'), respectively.

The diagrams which contribute to w_ξ are shown in Figs. 13(b-1)–13(b-5). We subtract contribution of Figs. 13(b-1') and 13(b-4'), which are fictitiously counted in Figs. 13(b-1) and 13(b-4), respectively. Thus we obtain

$$w_\xi = -2\tilde{g}_1\tilde{D}_\xi + \tilde{g}_2\tilde{D}_\xi + \tilde{D}_\eta\tilde{D}_\xi - \tilde{g}_2\tilde{D}_\eta\tilde{D}_\xi + \frac{1}{2}\tilde{g}_1\tilde{D}_\eta\tilde{D}_\xi$$

$$-2\tilde{D}_\xi^2 - \tilde{D}_\eta^2\tilde{D}_\xi. \tag{A12}$$

The first, second, . . . , seventh terms of the right-hand side come from Figs. 13(b-1), . . . , 13(b-5), 13(b-1'), and 13(b-4'), respectively. Expressions (27)–(31) and (32)–(37) complete the two-loop RG equations for the single-chain problem.
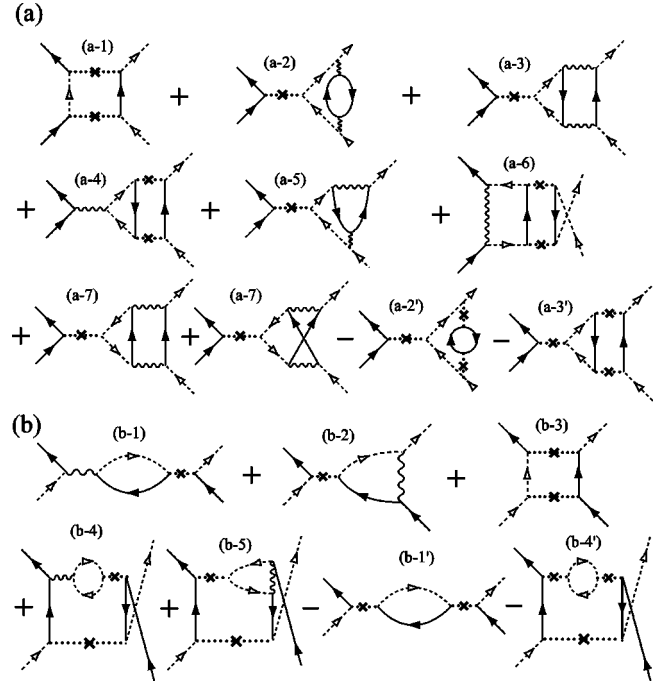

FIG. 13. Vertex correction diagrams which contribute to (a) w_η and (b) w_ξ

APPENDIX B: DERIVATION OF RG EQUATIONS FOR INTERCHAIN PROCESSES

Now, it is straightforward to extend the RG formulation in the single-chain problem to the case of the coupled chain problem. Integration over the modes in the high-energy shell gives, instead of Eq. (A1)

$$Z = \int_{\mathcal{C}_{l+dl}^<} \prod_\alpha^N \mathcal{D}_\alpha \exp\left[\sum_{\alpha=1}^N \left\{\tilde{S}_{l+dl}^{\alpha<} + \sum_{p,q,r,s,t=1}^\infty dS_{pqrst}^\alpha\right\}\right], \tag{B1}$$

where

$$dS_{pqrst}^\alpha = \frac{1}{p!q!r!s!t!}\langle\langle[S_{\mathrm{I};l+dl}^{\alpha>}]^p[S_{\eta;l+dl}^{\alpha>}]^q[S_{\xi;l+dl}^{\alpha>}]^r$$

$$\times[S_{1\perp;l+dl}^{\alpha>}]^s[S_{2\perp;l+dl}^{\alpha>}]^t\rangle\rangle_c. \tag{B2}$$

Here $S_{\mathrm{I};l}^\alpha$, $S_{\eta;l}^\alpha$, and $S_{\xi;l}^\alpha$ denote the two-particle interaction, random forward scattering, and random backward scattering terms of independent $N_\perp$ chains, respectively. Then the renormalized actions for the interchain processes are written in the forms

$$2\sum_{k_a\in\mathcal{C}_{l+dl}}\sum_{-\pi\leqslant k_b,k_c\leqslant\pi}\sum_\varepsilon\sum_\sigma t_\perp(\cos k_b + \cos k_c)$$

$$\times[L_\sigma^{\alpha*}(K)L_\sigma^\alpha(K) + R_\sigma^{\alpha*}(K)R_\sigma^\alpha(K)] \tag{B3}$$

and

$$- \frac{\pi v_F}{N_\perp} \sum_Q [J_{q_\perp} + w^J_{q_\perp} dl] S^\alpha_{l+dl}(Q) \cdot S^\alpha_{l+dl}(-Q)$$

$$- \frac{\pi v_F}{N_\perp} \sum_Q [K_{q_\perp} + w^K_{q_\perp} dl]$$

$$\times [S^\alpha_{l+dl}(2k_F + q_a, q_\perp, i\omega)$$

$$\cdot S^\alpha_{l+dl}(2k_F - q_a, -q_\perp, -i\omega) + \text{c.c.}], \quad (B4)$$

corresponding to $S^{\alpha>}_{1\perp;l}$ and $S^{\alpha>}_{2\perp;l}$, respectively. The first and second terms of the expression (B4) correspond to Figs. (14a) and (14b), respectively.

Next, we rescale the momenta and frequencies as $\hat{K} = (e^{dl} k_a, k_\perp, e^{dl} i\varepsilon)$, with $k_\perp = (k_b, k_c)$ and $\hat{Q} = (e^{dl} q_a, q_\perp, e^{dl} i\omega)$, and perform the field renormalization

$$\hat{R}(\hat{K}) = \left(1 + \frac{\theta - 3}{2} dl\right) R(K).$$

In the rescaling procedure, $k_\perp$ and $q_\perp$ are *not* rescaled, because in the energy scale considered here the one-particle thermal coherence length across the chains becomes comparable to the distance between the adjacent chains and, consequently, the scaling procedure is invalid in the direction perpendicular to the chains. Then the renormalized action for the interchain processes takes the forms

$$2 \sum_{\hat{k}_a \in C_l} \sum_{-\pi \leq k_b, k_c \leq \pi} \sum_{\hat{\varepsilon}} \sum_\sigma (1 - \theta dl) t_\perp (\cos k_b + \cos k_c)$$

$$\times [\hat{L}^{\alpha*}_\sigma(\hat{K}) \hat{L}^\alpha_\sigma(\hat{K}) + \hat{R}^{\alpha*}_\sigma(\hat{K}) \hat{R}^\alpha_\sigma(\hat{K})], \quad (B5)$$
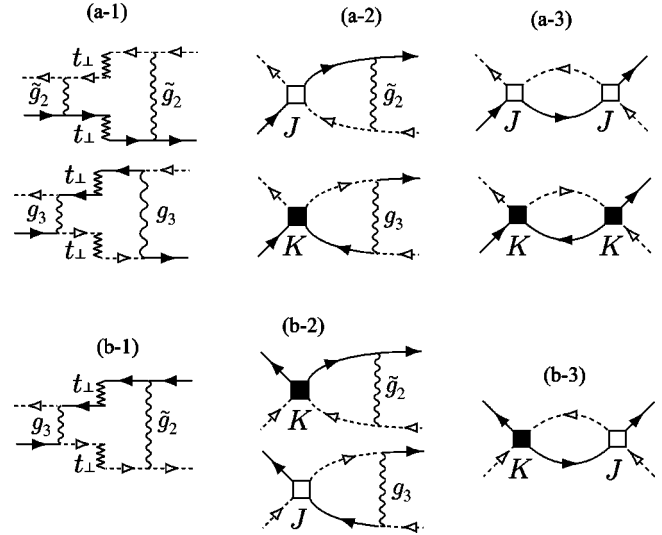
and

FIG. 14. Renormalization of the ICEX processes in the AF channel for the (a) normal and (b) umklapp processes.

$$\tilde{S}^\alpha_{2\perp;l} = - \frac{\pi v_F}{N_\perp} \sum_{\hat{Q}} [J_{q_\perp} + (w^J_{q_\perp} - 2\theta J_{q_\perp}) dl] \hat{S}^\alpha_l(\hat{Q}) \cdot \hat{S}^\alpha_l(-\hat{Q})$$

$$- \frac{\pi v_F}{N_\perp} \sum_{\hat{Q}} [K_{q_\perp} + (w^K_{q_\perp} - 2\theta K_{q_\perp}) dl]$$

$$\times [\hat{S}^\alpha_l(2\hat{k}_F + \hat{q}_a, q_\perp, i\hat{\omega})$$

$$\cdot \hat{S}^\alpha_l(2\hat{k}_F - \hat{q}_a, -q_\perp, -i\hat{\omega}) + \text{c.c.}], \quad (B6)$$

corresponding to $S^{\alpha>}_{1\perp;l}$ and $S^{\alpha>}_{2\perp;l}$, respectively. Thus we have reached the RG equations for the interchain processes, Eqs. (48)–(50).

[1] *Electron-Electron Interactions in Disordered Systems*, edited by A. L. Efros and M. Pollak (Elsevier, Amsterdam, 1985).

[2] P. A. Lee and T. V. Ramakrishnan, Rev. Mod. Phys. **57**, 287 (1985).

[3] *Anderson Localization*, edited by Y. Nagaoka [Prog. Theor. Phys. Suppl. **84**, 1 (1985)].

[4] D. Belitz and T. R. Kirkpatrick, Rev. Mod. Phys. **66**, 261 (1994).

[5] T. Saso, Y. Suzumura, and H. Fukuyama, Prog. Theor. Phys. Suppl. **84**, 269 (1985).

[6] T. Giamarchi and H. J. Schulz, Phys. Rev. B **37**, 325 (1988).

[7] S. Fujimoto and N. Kawakami, Phys. Rev. B **54**, 11 018 (1996).

[8] E. Orignac, T. Giamarchi, and P. Le Doussal, Phys. Rev. Lett. **83**, 2378 (1999).

[9] A. A. Abrikosov, Phys. Rev. B **50**, 1415 (1994).

[10] N. Dupuis and G. Montambaux, Phys. Rev. B **46**, 9603 (1992).

[11] C. Mauz, A. Rosch, and P. Wölfle, Phys. Rev. B **56**, 10 953 (1997).

[12] Y. Nakamura and H. Fukuyama, J. Phys. Soc. Jpn. **67**, 1371 (1998).

[13] S. A. Brazovskii and V. M. Yakovenko, Zh. Éksp. Teor. Fiz. **89**, 2318 (1985) [Sov. Phys. JETP **62**, 1340 (1985)].

[14] C. Bourbonnais and L. G. Caron, Int. J. Mod. Phys. B **5**, 1033 (1991).

[15] C. Bourbonnais, in *Strongly Interacting Fermions and High T_c Super-conductivity*, edited by B. Doucot and J. Zin-Justin (Elsevier, Amsterdam, 1995), p. 307.

[16] C. Bourbonnais, J. Phys. I **3**, 143 (1993).

[17] J. Kishine and K. Yonemitsu, J. Phys. Soc. Jpn. **67**, 2590 (1998).

[18] J. Kishine and K. Yonemitsu, J. Phys. Soc. Jpn. **68**, 2790 (1999).

[19] J. Kishine and K. Yonemitsu Mol. Cryst. Liq. Cryst. Sci. Technol., Sect. A **341**, 555 (2000).

[20] T. Giamarchi and B. S. Shastry, Phys. Rev. B **51**, 10 915 (1995).

[21] T. Itoh, Master thesis, University of Tokyo, 2000; T. Itoh, K. Hiraki, and K. Kanoda (private communication).

[22] K. Ueda and T. M. Rice, Phys. Rev. B **29**, 1514 (1984).

[23] J. Kishine, Phys. Rev. B **62**, 2377 (2000).

[24] J. Sólyom, Adv. Phys. **28**, 201 (1979).

[25] D. Boies, C. Bourbonnais, and A.-M. S. Tremblay, Phys. Rev. Lett. **74**, 968 (1995).

[26] K. Hiraki and K. Kanoda, Phys. Rev. B **54**, 17 276 (1996).

[27] See H. J. Schulz, in *Strongly Correlated Electronic Materials*, edited by K. S. Bedell, Z. Q. Wang, D. e. Meltzer, A. V. Balatsky, and E. Abrahams (Addison-Wesley, Reading, MA, 1994), p. 187.

[28] K. Yonemitsu, Phys. Rev. B **56**, 7262 (1997).

[29] M. Fabrizio, Phys. Rev. B **48**, 15 838 (1993).

[30] T. Giamarchi and H. J. Schulz, J. Phys. (Paris) **49**, 819 (1988).

[31] Y. Suzumura, M. Tsuchiizu, and G. Grüner, Phys. Rev. B **57**, 15 040 (1998).